

MonoMAE: Enhancing Monocular 3D Detection through Depth-Aware Masked Autoencoders

Xueying Jiang¹, Sheng Jin¹, Xiaoqin Zhang², Ling Shao³, and Shijian Lu¹✉

¹ Nanyang Technological University

² College of Computer Science and Technology, Zhejiang University of Technology

³ UCAS-Terminus AI Lab, UCAS

Abstract. Monocular 3D object detection aims for precise 3D localization and identification of objects from a single-view image. Despite its recent progress, it often struggles while handling pervasive object occlusions that tend to complicate and degrade the prediction of object dimensions, depths, and orientations. We design MonoMAE, a monocular 3D detector inspired by Masked Autoencoders that addresses the object occlusion issue by masking and reconstructing objects in the feature space. MonoMAE consists of two novel designs. The first is depth-aware masking that selectively masks certain parts of non-occluded object queries in the feature space for simulating occluded object queries for network training. It masks non-occluded object queries by balancing the masked and preserved query portions adaptively according to the depth information. The second is lightweight query completion that works with the depth-aware masking to learn to reconstruct and complete the masked object queries. With the proposed object occlusion and completion, MonoMAE learns enriched 3D representations that achieve superior monocular 3D detection performance qualitatively and quantitatively for both occluded and non-occluded objects. Additionally, MonoMAE learns generalizable representations that can work well in new domains.

Keywords: Monocular 3D Object Detection · Masked Autoencoders · Occlusion

1 Introduction

3D object detection has emerged as one key component in various navigation tasks such as autonomous driving, robot patrolling, etc. Compared with prior studies relying on LiDAR [23, 56, 60] or multi-view images [24, 27, 53], monocular 3D object detection offers a more cost-effective and accessible alternative which identifies objects and predicts their 3D locations from single-view images. On the other hand, monocular 3D object detection is much more challenging due to the lack of 3D information from multi-view images or LiDAR data.

Among various new challenges in monocular 3D detection, object occlusion, which exists widely in natural images as illustrated in Figure 1 (a), becomes a critical issue while predicting 3D location in terms of object depths, object

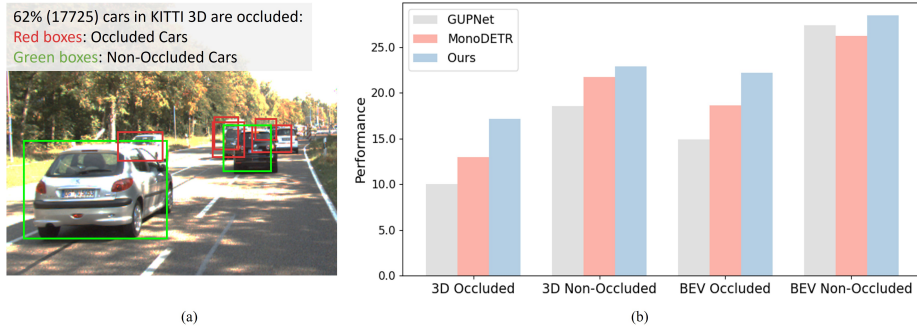


Fig. 1: Object occlusion is pervasive and affects monocular 3D detection: Object occlusion is pervasive, e.g., 62% (17725) cars in the KITTI 3D dataset suffer from various occlusions as illustrated in (a). Prevalent monocular 3D detection techniques such as GUPNet [31] and MonoDETR [57] are clearly affected by object occlusions in both 3D space (3D) and the bird’s eye view (BEV) space as in (b). Our MonoMAE simulates and learns object occlusions by feature masking and completing which improves detection consistently for both occluded and non-occluded objects.

dimensions, and object orientations. Most existing monocular 3D detectors such as MonoDETR [57] and GUPNet [31] neglect the object occlusion issue which demonstrates clear performance degradation as illustrated in Figure 1 (b). A simple idea is to learn to reconstruct the occluded object regions whereby occluded objects can be handled similarly as non-occluded objects. On the other hand, reconstructing occluded object regions in the image space is complicated due to the super-rich variation of object occlusions in scene images.

Inspired by the Masked Autoencoders (MAE) [15] that randomly occludes image patches and reconstructs them in representation learning, we treat object occlusions as natural masking and train networks to complete occluded object regions to learn occlusion-tolerant representations. To this end, we design MonoMAE, a novel monocular 3D detection framework that adopts the idea of MAE by first masking certain object regions in the feature space (for simulating object occlusions) and then reconstructing the masked object features (for learning occlusion-tolerant representations). MonoMAE consists of a depth-aware masking module and a lightweight completion network. The depth-aware masking simulates object occlusions by masking the features of non-occluded objects adaptively according to the object depth information. It generates pairs of non-occluded and masked (i.e., occluded) object representations that can be directly applied to train the lightweight completion network, aiming for completing the occluded objects and learning occlusion-tolerant representations. Note that MonoMAE introduces little computational overhead in inference time as it requires no object masking in the inference stage and the completion network is lightweight. Moreover, completion in the feature space can be effectively achieved using a lightweight network, surpassing the complex encoder-decoder structure required for image space completion.

The contributions of this work can be summarized in three major aspects. *First*, we design MonoMAE, a MAE-inspired monocular 3D detection framework that tackles object occlusions effectively by masking and reconstructing object regions at the feature level. *Second*, we design adaptive image masking and a lightweight completion network that mask non-occluded objects adaptively according to the object depth (for simulating object occlusions) and reconstruct the masked object (for learning occlusion-tolerant representations), respectively. *Third*, extensive experiments over KITTI 3D and nuScenes show that MonoMAE outperforms the state-of-the-art consistently and it can generalize to new domains as well.

2 Related Work

2.1 Monocular 3D Object Detection

Monocular 3D detection aims for identification and 3D localization of objects from a single-view image. Most existing work can be broadly classified into two categories. The first employs convolutional neural networks and most methods adopt center-guided pipelines following conventional 2D detectors [12]. The standard approach learns monocular 3D detectors from single-view images only [1, 8, 17, 57, 61]. To acquire more depth information, several studies explore to leverage extra training data, such as LiDAR point clouds [6, 33, 41, 48], depth maps [11, 21, 39, 40], and 3D CAD models [7, 29, 36]. Beyond that, several studies exploit the geometry relation between 2D and 3D spaces in different ways. For example, M3D-RPN [1] applies the powerful 2D detector FPN [42] for 3D detection. MonoDLE [34] aligns the centers of 2D and 3D boxes for better 3D localization. GUPNet [31] leverages uncertainty modeling to estimate the height of 3D boxes from the 2D boxes.

The second introduces powerful visual transformers for more accurate monocular 3D detection [19, 49, 50, 57, 62]. For example, MonoDTR [19] integrates context- and depth-aware features and injects depth positional hints into transformers. MonoDETR [57] modifies the transformer to be depth-aware and guides the detection process by contextual depth cues. However, most existing studies neglect object occlusions that exist widely in natural images and often degrade the performance of monocular 3D object detection clearly. We adopt the transformer architecture to learn occlusion-tolerant representations that can handle object occlusion effectively without requiring any extra data.

2.2 Occlusions in 3D Object Detection

Object occlusion is pervasive in scene images and it has been investigated in several 3D detection studies [8, 10, 18, 25, 45, 52, 55]. One typical approach learns to estimate the complete localization of occluded objects. For example, Mono3DT [18] estimates complete 3D bounding boxes by re-identifying occluded vehicles from a sequence of 2D images. BtcDet [52] leverages object shape priors

and learns to estimate the complete shapes of partially occluded objects. Several studies consider the degree of occlusions in training. For example, MonoPair [8] exploits the relation of paired samples and encodes spatial constraints of occluded objects from their neighbors. HMF [25] introduces an anti-occlusion loss to focus on occluded samples. Different from previous methods, our MonoMAE learns enriched and occlusion-tolerant representations by masking and completing object parts in the feature space.

2.3 Masked Autoencoders in 3D Tasks

Masked Autoencoders (MAE) [15] learn visual representations by masking image patches and reconstructing them, and it has been explored in several point cloud pre-training studies. For outdoor point cloud pre-training, Occupancy-MAE [35] exploits range-aware random masking that employs three masking levels to deal with the sparse voxel occupancy structures of LiDAR point clouds. GD-MAE [54] introduces a Generative Decoder to merge the surrounding context to restore the masked tokens hierarchically. For indoor point cloud pre-training, PointMAE [37] adopts MAE to directly reconstruct the 3D coordinates of masked tokens. I2P-MAE [58] introduces 2D pre-trained models which enhances 3D pre-training with diverse 2D semantics. PiMAE [5] learns cross-modal representations with MAE by interactively handling point clouds and RGB images. Different from the above studies, our MonoMAE handles monocular 3D detection from single-view images and it focuses on object occlusions by learning to complete occluded object regions at the feature level.

3 Proposed Method

3.1 Problem Definition

Monocular 3D detection takes a single RGB image as input, aiming to classify objects and predict their 3D bounding boxes. The prediction of each object is composed of the object category C , a 2D bounding box B_{2D} , and a 3D bounding box B_{3D} where B_{3D} can be further decomposed to the object 3D location (x_{3D}, y_{3D}, z_{3D}) , the object dimensions in object height, width and length (h_{3D}, w_{3D}, l_{3D}) , as well as the object orientation θ .

3.2 Overall Framework

Figure 2 shows the framework of the proposed MonoMAE. Given an input image I , the 3D Backbone first generates a sequence of 3D object queries $Q = [q_1, q_2, \dots, q_K]$ (K denotes query number) and the Non-Occluded Query Grouping then classifies the queries into two groups including non-occluded queries $Q^{NO} = [q_1^{NO}, q_2^{NO}, \dots, q_U^{NO}]$ and occluded queries $Q^O = [q_1^O, q_2^O, \dots, q_V^O]$ (U and V are the number of non-occluded and occluded queries). The Non-Occluded Query Masking then masks Q^{NO} to produce masked queries according to their

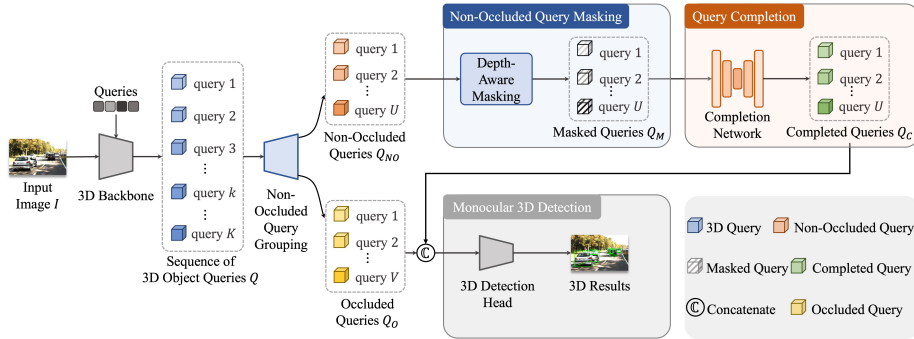


Fig. 2: The training framework: Given a single-view image, the 3D Backbone extracts 3D object query features which are grouped into non-occluded query features and occluded query features by the Non-Occluded Query Grouping. The Depth-Aware Masking then masks the non-occluded query features to simulate object occlusions according to the object depth, and the Completion Network further learns to reconstruct the masked queries. Finally, the completed and the occluded query features are concatenated to train the 3D Detection Head for 3D predictions.

depth $D = [d_1, d_2, \dots, d_U]$, leading to the masked queries $Q^M = [q_1^M, q_2^M, \dots, q_U^M]$. The Query Completion further reconstructs Q^M to produce the completed queries $Q^C = [q_1^C, q_2^C, \dots, q_U^C]$. Finally, the occluded queries Q^O and the completed queries Q^C are concatenated and fed to the Monocular 3D Detection for 3D detection predictions. Note the inference does not involve the Non-Occluded Query Masking, and it just concatenates the completion of occluded queries Q^O (i.e., Q^C) with the non-occluded queries Q^{NO} and feeds the concatenated queries to the 3D Detection Head for 3D predictions as illustrated in Figure 3.

3.3 Non-Occluded Query Masking

Queries predicted by the 3D Backbone are either occluded or non-occluded, depending on whether the corresponding objects are occluded in the input image. In MonoMAE, we mask the non-occluded queries in the feature space to simulate occlusions, aiming to generate pairs of non-occluded and masked (i.e., occluded) queries for learning occlusion-tolerant object representations. Specifically, we design Non-Occluded Query Grouping to identify non-occluded queries and feed them into the Depth-Aware Masking to synthesize occlusions.

Specifically, we design a Non-Occluded Query Grouping module to identify non-occluded queries and then feed them into a designed Depth-Aware Masking module to synthesize occlusions, with more detail to be elaborated in the following subsections.

Non-Occluded Query Grouping. The Non-Occluded Query Grouping classifies the queries based on whether their corresponding objects are occluded or non-occluded. With no information about whether the input queries are occluded, we design an occlusion classification network Φ_O to predict the occlusion

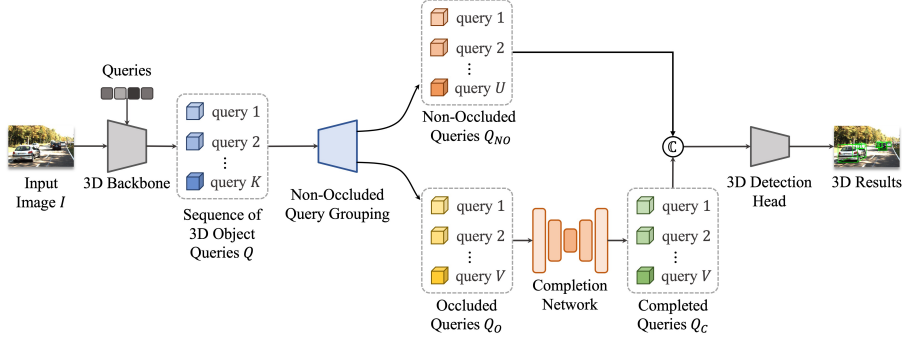


Fig. 3: The inference framework. Given a test image, the 3D Backbone extracts 3D object queries and feeds the queries to the Non-Occluded Query Grouping for classification. The identified *occluded* queries are then fed to the Completion Network to reconstruct the *completed* queries. Finally, the *completed* queries and the identified *non-occluded* queries are concatenated and fed to the 3D Detection Head for 3D detection predictions.

condition $O^p = [o_1^p, o_2^p, \dots, o_K^p]$ of queries $Q = [q_1, q_2, \dots, q_K]$, where for the i -th query $o_i^p = \Phi_O(q_i)$. The Non-Occluded Query Grouping can be formulated by:

$$\begin{cases} q_i \in Q^{NO} & \text{if } o_i^p = 0 \\ q_i \in Q^O & \text{if } o_i^p = 1 \end{cases}, \quad (1)$$

where $o_i^p = 0$ denotes the query is non-occluded, and $o_i^p = 1$ denotes the query is occluded. The occlusion classification network is trained with the occlusion classification loss L_{occ} as follows:

$$L_{occ} = CE(O^p, O^{gt}), \quad (2)$$

where CE is the *Cross Entropy* loss. We adopted the bipartite matching [4] to match the predicted queries and objects in the image, where only matched queries have ground truth O^{gt} of KITTI 3D [13] about whether they are occluded or not. Please refer to the supplementary materials for details.

Depth-Aware Masking. We design depth-aware masking to adaptively mask non-occluded query features to simulate occlusions at the feature level, aiming to create non-occluded and occluded (i.e., masked) pairs for learning occlusion-tolerant representations. As illustrated in Figure 4, the depth-aware masking determines the mask ratio according to the object depth - the closer the object, the larger the mask ratio, thereby compensating the information deficiency of distant objects. In addition, we simulate occlusions by masking at the feature level, as masking and reconstructing at the image level is complicated and computationally intensive.

The depth-aware masking first obtains the query depth before query masking. Without backward gradient propagation, it adopts the 3D Detection Head to obtain the depth $D = [d_1, d_2, \dots, d_U]$ for non-occluded queries. With the

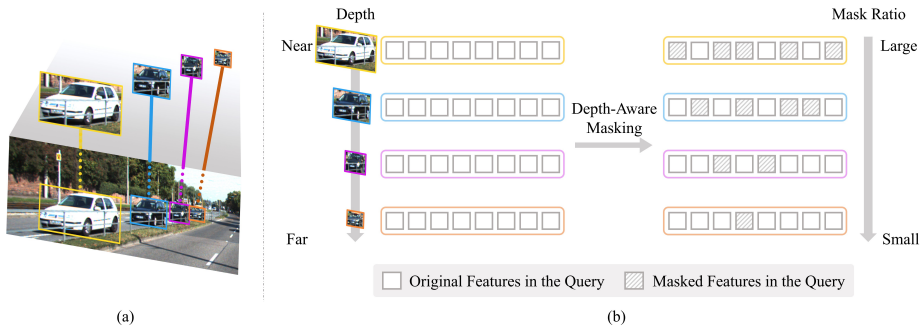


Fig. 4: Illustration of the Depth-Aware Masking. (a) Objects farther away are usually smaller with less visual information. (b) The Depth-Aware Masking determines the mask ratio of an object according to its depth - the closer the object is, the larger the mask ratio is applied, thereby compensating the information deficiency for objects that are distant from the camera.

predicted depth, each non-occluded query is randomly masked as illustrated in Figure 4. Specifically, objects that are more distant from the camera are usually captured with less visual information. The depth-aware masking accommodates this by assigning a smaller masking ratio to them, thereby keeping more visual information for distant objects for proper visual representation learning.

The mask ratio r of each query is determined by:

$$r = 1.0 - d_i/D_{max}, \quad (3)$$

where r is the applied mask ratio for each query, d_i is the depth for the i -th query, and D_{max} is the maximum depth in datasets. The masks $M = [m_1, m_2, \dots, m_U]$ generated for queries obey a Bernoulli Distribution.

Finally, the query masking is formulated by:

$$q_i^M = q_i^{NO} * m_i, \quad (4)$$

where q_i^M is the i -th masked query, q_i^{NO} is the i -th non-occluded query, and m_i is the generated mask.

3.4 Query Completion

The query completion learns to reconstruct the adaptively masked queries, aiming to produce completed queries whereby the network learns occlusion-tolerant representations that are helpful in detecting occluded objects. We design a completion network Φ_C to reconstruct the masked queries. The Completion Network has an hourglass structure consisting of three conv-bn-relu blocks and one conv-bn block for 3D query completion. Please refer to the appendix for details. The completed query q_i^C is obtained by:

$$q_i^C = \Phi_C(q_i^M), \quad (5)$$

where q_i^M is the masked query. The Completion Network is trained under the supervision of the non-occluded queries before masking, where a completion loss L_{com} is formulated as follows:

$$L_{com} = L_1^s(Q^{NO}, Q^C), \quad (6)$$

where L_1^s denotes the SmoothL1 loss [14], Q^{NO} denotes the non-occluded queries, and Q^C denotes the queries completed by the Completion Network.

3.5 Loss Functions

The overall objective consists of three losses including L_{occ} , L_{com} , and L_{base} where L_{occ} and L_{com} are defined in Equation 2 and Equation 6, and L_{base} denote losses for supervising the 3D box predictions.

L_{base} includes losses for supervising the 3D box predictions including each object’s 3D locations, height, width, length and orientation. We set the weight for each loss item to 1.0, and the overall loss function is formulated as follows:

$$L = L_{occ} + L_{com} + L_{base}. \quad (7)$$

4 Experiments

4.1 Experimental Settings

Datasets. We benchmark our method over two public datasets in monocular 3D object detection.

- KITTI 3D [13] comprises 7,481 training images and 7,518 testing images, with training-data labels publicly available and test-data labels stored on a test server for evaluation. Following [7], we divide the 7,481 training samples into a new train set with 3,712 images and a validation set with 3,769 images for ablation studies.

- NuScenes [3] comprises 1,000 video scenes, including RGB images captured by 6 surround-view cameras. The dataset is split into a training set (700 scenes), a validation set (150 scenes), and a test set (150 scenes).

Following [1, 20, 22, 31, 43], the performance on the validation set is reported. We follow prior studies [43, 44, 47, 57] that evaluate only on the most representative Car category of KITTI 3D and nuScenes datasets.

Evaluation Metrics. For KITTI 3D, we follow [44] and adopt $AP|_{R_{40}}$, the average of the AP of 40 recall points as the evaluation metric. We report the average precision on BEV and 3D object detection by $AP_{BEV}|_{R_{40}}$ and $AP_{3D}|_{R_{40}}$ with a threshold of 0.7 for both test and validation sets. For the nuScenes dataset, we adopt the mean absolute depth errors [43] for evaluations.

Implementation Details. We conduct experiments on one NVIDIA V100 GPU and train the framework for 200 epochs with a batch size of 16 and a

Table 1: Benchmarking on the KITTI 3D *test* set. All experiments adopt $AP|_{R_{40}}$ metric with an IoU threshold of 0.7. Best in **bold**, second underlined.

Method	Venue	Extra Data	$AP_{3D}(IoU=0.7) _{R_{40}}$			$AP_{BEV}(IoU=0.7) _{R_{40}}$			
			Easy	Moderate	Hard	Easy	Moderate	Hard	
MonoRUn [6]	CVPR 21	LiDAR	19.65	12.30	10.58	27.94	17.34	15.24	
CaDDN [41]	CVPR 21		19.17	13.41	11.46	27.94	18.91	17.19	
MonoDTR [19]	CVPR 22		21.99	15.39	12.73	28.59	20.38	17.14	
MonoDistill [9]	ICLR 22		22.97	16.03	13.60	31.87	22.59	19.72	
DID-M3D [39]	ECCV 22		24.40	16.29	13.75	32.95	22.76	19.83	
MonoNeRD [51]	ICCV 23		22.75	17.13	<u>15.63</u>	31.13	<u>23.46</u>	<u>20.97</u>	
PatchNet [32]	ECCV 20	Depth	15.68	11.12	10.17	22.97	16.86	14.97	
D4LCN [11]	CVPR 20		16.65	11.72	9.51	22.51	16.02	12.55	
DDMP-3D [46]	CVPR 21		19.71	12.78	9.80	28.08	17.89	13.44	
DD3D [38]	ICCV 21		23.22	16.34	14.20	30.98	22.56	20.03	
MonoPGC [49]	ICRA 23		24.68	<u>17.17</u>	14.14	32.50	23.14	20.30	
Kinematic3D [2]	ECCV 20	Video	19.07	12.72	9.17	26.69	17.52	13.10	
AutoShape [29]	ICCV 21	CAD	22.47	14.17	11.36	30.66	20.08	15.59	
M3D-RPN [1]	ICCV 19	None	14.76	9.71	7.42	21.02	13.67	10.23	
SMOKE [28]	CVPRW 20		14.03	9.76	7.84	20.83	14.49	12.75	
MonoPair [8]	CVPR 20		13.04	9.99	8.65	19.28	14.83	12.89	
MonoDLE [34]	CVPR 21		17.23	12.26	10.29	24.79	18.89	16.00	
MonoFlex [59]	CVPR 21		19.94	13.89	12.07	28.23	19.75	16.89	
MonoRCNN [43]	ICCV 21		18.36	12.65	10.03	25.48	18.11	14.10	
GUPNet [31]	ICCV 21		20.11	14.20	11.77	-	-	-	
DEVIANT [22]	ECCV 22		21.88	14.46	11.89	29.65	20.44	17.43	
MonoCon [26]	AAAI 22		22.50	16.46	13.95	31.12	22.10	19.00	
MonoDETR [57]	ICCV 23		<u>25.00</u>	16.47	13.58	<u>33.60</u>	22.11	18.60	
MonoUNI [20]	NeurIPS 23		24.75	16.73	13.49	-	-	-	
Ours	-		None	25.60	18.84	16.78	34.15	24.93	21.76

learning rate of 2×10^{-4} . We use the AdamW [30] optimizer with weight decay 10^{-4} . We employ ResNet-50 [16] as the Transformer-based backbone and adopt the 3D detection head from [57] for our framework.

4.2 Benchmarking with the State-of-the-Art

We benchmark MonoMAE with state-of-the-art monocular 3D object detection methods both quantitatively and qualitatively.

Quantitative Benchmarking. We conducted quantitative benchmarking over the Car category of the test set on KITTI 3D as shown in Table 1, where all evaluations were performed on the official online test server [13] for fairness. We can see that MonoMAE achieves superior detection performance consistently across all metrics, without using any extra training data such as image depths, video sequences, LiDAR points, and CAD 3D models. In addition, MonoMAE outperforms more for the Moderate and Hard categories where various occlusions happen much more frequently than the Easy category. The superior performance



Fig. 5: Detection visualization over the KITTI *val* set. Ground-truth annotations are highlighted by red boxes, and predictions by MonoMAE and two state-of-the-art methods are highlighted by green boxes. Red arrows highlight objects that have very different predictions across the compared methods. The ground truth of LiDAR point clouds is provided for visualization only, and they are not used in MonoMAE training. Best viewed in color and zoom-in.

is largely attributed to our designed depth-aware masking and completion network which masks queries to simulate object occlusions in the feature level and reconstructs the masked queries to learn occlusion-tolerant visual representations, respectively.

Qualitative Benchmarking. Figure 5 shows qualitative benchmarking on the KITTI 3D *val* set. It can be observed that compared with two state-of-the-art methods GUPNet and MonoDETR, our MonoMAE produces more accurate

Table 2: Ablation study of technical designs in MonoMAE on the KITTI 3D *val* set. ‘NOQG’, ‘DAM’, and ‘CN’ denote the Non-Occluded Query Grouping, the Depth-Aware Masking, and the Completion Network, respectively. The symbol * indicates the baseline. The best results are highlighted in **bold**.

Index	NOQG	DAM	CN	AP _{3D} (IoU= 0.7) _{R40}			AP _{BEV} (IoU= 0.7) _{R40}		
				Easy	Moderate	Hard	Easy	Moderate	Hard
1*	✓			24.85	16.21	14.74	34.53	23.99	18.84
2		✓		23.33	15.09	13.20	32.68	21.80	17.43
3			✓	27.33	18.52	14.95	36.51	24.21	19.12
4	✓	✓		24.69	15.71	13.57	33.46	23.03	18.19
5	✓		✓	27.25	18.76	15.45	36.81	25.18	20.05
6		✓	✓	28.39	19.35	15.87	37.59	26.27	21.33
7	✓	✓	✓	30.29	20.90	17.61	40.26	27.08	23.14

Table 3: Ablation study of three masking strategies on the KITTI 3D *val* set. The best results are highlighted in **bold**.

Index	Masking Strategy	AP _{3D} (IoU= 0.7) _{R40}			AP _{BEV} (IoU= 0.7) _{R40}		
		Easy	Moderate	Hard	Easy	Moderate	Hard
1	Image Masking	20.51	15.03	13.24	27.76	19.74	16.71
2	Query Masking (w/o Depth-Aware)	27.14	18.47	15.02	36.98	25.52	20.64
3	Query Masking (w/ Depth-Aware)	30.29	20.90	17.61	40.26	27.08	23.14

3D detection consistently for both non-occluded and occluded objects, even for some hard scenarios like distant objects. Specifically, GUPNet and MonoDETR tend to miss the detection of highly occluded object in Cases 1 and 2 as highlighted by red arrows, while our MonoMAE performs clearly better by detecting those challenging objects successfully, demonstrating its superior capability on handling object occlusions. More visualization results can be found in supplementary materials.

4.3 Ablation Study

We conduct extensive ablation studies to examine our proposed MonoMAE. Specifically, we examine MonoMAE from the aspect of the technical designs, query mask approaches, as well as loss functions.

Network Designs. We examine the effectiveness of two key designs in MonoMAE, namely, the Depth-Aware Masking module (DAM) and the Completion Network (CN) (on the test set of KITTI 3D). We formulate the baseline by including the Non-Occluded Query Grouping module (NOQG), which does not affect the network training as both identified occluded and non-occluded queries are fed to train 3D detectors. While incorporating DAM only in Rows 2 and 4, the 3D detection degrades clearly as queries are masked but not reconstructed which leads to further information loss. While incorporating CN alone in Rows 3 and 5, the detection improves clearly as the completion helps learn better

Table 4: Ablation study of the loss functions on the KITTI 3D *val* set. L_{occ} and L_{com} refer to the occlusion classification loss and the completion loss, respectively. The best results are highlighted in **bold**.

Index	L_{occ}	L_{com}	AP _{3D} (IoU= 0.7) _{R40}			AP _{BEV} (IoU= 0.7) _{R40}		
			Easy	Moderate	Hard	Easy	Moderate	Hard
1	✓		28.37	19.61	16.01	37.48	26.55	21.50
2		✓	26.36	19.15	15.88	36.76	26.49	22.62
3	✓	✓	30.29	20.90	17.61	40.26	27.08	23.14

representations for naturally occluded queries. In addition, incorporating DAM and CN on top of NOQG in Row 7 performs clearly better than incorporating DAM and CN alone in Row 6, as the former applies masking and completion to non-occluded queries only. It also shows that masking naturally occluded queries to train the completion network is harmful to the learned representations.

Masking Strategies. We examine how different masking strategies affect monocular 3D detection. We studied three masking strategies as shown in Table 3. The first strategy masks the *input images* randomly, aiming to assess the value of masking and completing at the feature instead of image level. We can observe that the image-level masking yields clearly lower performance as compared with query masking in the feature space, largely due to the complication in masking and reconstructing images with a lightweight completion network. The second strategy masks query features randomly without considering object depths, aiming to evaluate the importance of object depths in query masking. The experiments show that random query masking outperforms the image-level masking significantly. The third strategy performs the proposed depth-aware query masking. It outperforms random query masking consistently, demonstrating the value of incorporating object depth information in query masking.

Loss Functions. We examine the impact of the occlusion classification loss L_{occ} and the completion loss L_{com} in Equation 2 and 6, where L_{occ} supervises the occlusion classification network (in Non-Occluded Query Grouping) to predict whether the queries are occluded and L_{com} supervises the Completion Network to reconstruct the masked queries. As Table 4 shows, while implementing L_{occ} alone, the occlusion prediction is supervised while the query reconstruction is unsupervised. The network under such an objective does not learn well as the Completion Network cannot reconstruct object queries well without sufficient supervision. While implementing L_{com} alone, the occlusion classification network cannot identify occluded and non-occluded queries accurately where many occluded queries are fed for masking, leading to more query occlusion and poor detection performance. While employing both losses concurrently, the performance improves significantly as non-occluded queries can be identified for masking and reconstruction, leading to occlusion-tolerant representations.

Table 5: Comparison on inference speed of several monocular 3D detection methods. Ours* denotes the proposed MonoMAE without including the Completion Network.

Method	GUPNet [31]	MonoDTR [19]	MonoDETR [57]	Ours*	Ours
Inference Time (ms)	40	37	43	36	38

Table 6: Cross-dataset evaluations that perform training on the KITTI train set, and testing on the KITTI val and nuScenes val sets. We adopt the evaluation metric mean absolute error of the depth (\downarrow). Best is highlighted in **bold**, and second underlined.

Method	KITTI Val				nuScenes frontal Val			
	0-20	20-40	40- ∞	All	0-20	20-40	40- ∞	All
M3D-RPN [1]	0.56	1.33	2.73	1.26	0.94	3.06	10.36	2.67
MonoRCNN [43]	0.46	1.27	2.59	1.14	0.94	2.84	8.65	2.39
GUPNet [31]	0.45	1.10	1.85	0.89	0.82	1.70	6.20	1.45
DEVIANT [22]	0.40	1.09	1.80	<u>0.87</u>	0.76	<u>1.60</u>	4.50	1.26
MonoUNI [20]	<u>0.38</u>	<u>0.92</u>	<u>1.79</u>	<u>0.87</u>	<u>0.72</u>	1.79	4.98	1.43
MonoMAE (Ours)	0.36	0.91	1.74	0.86	0.71	1.57	<u>4.95</u>	<u>1.40</u>

4.4 Discussions

Efficiency Comparison. We compare the inference time of several representative monocular 3D detection methods on the KITTI val set, where all compared methods are evaluated with one NVIDIA V100 GPU under the same computational environment for fairness. As Table 5 shows, GUPNet, MonoDTR, and MonoDETR have an average inference time of 40ms, 37ms, and 43ms for each image, respectively. As a comparison, the proposed MonoMAE takes the shortest inference time, demonstrating its good efficiency in monocular 3D detection. The good efficiency can be attributed to several factors. First, MonoMAE does not involve Depth-Aware Masking but just the Completion Network for reconstructing occluded queries. In addition, the Completion Network is lightweight which just introduces 2ms computational overhead as shown in the last two columns of Table 5. Further, we analyzed the Completion Network in terms of network parameters and floating-point operations per second (FLOPs), showing that it has very limited 2.22G parameters and 0.08M in FLOPs.

Generalization Ability. We examine the generalization capability of the proposed MonoMAE by directly applying the KITTI-trained MonoMAE model to the car Category of the nuScenes validation set without additional training. The performance on the KITTI validation set is also reported for reference. Table 6 illustrates that MonoMAE attains the highest or second-highest performance across various metrics on the nuScenes frontal validation set. This indicates that despite the domain shift from KITTI to nuScenes, MonoMAE still maintains satisfactory performance. DEVIANT [22] also achieves great monocular 3D detection performance on nuScenes as it treats objects of different depths equally and is thus robust to depth variations.

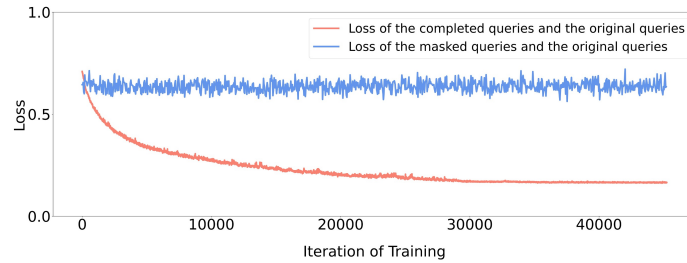


Fig. 6: Completion Network validation with loss visualization. The **red** curve shows the loss of the original queries and completed queries by the Completion Network. The **blue** curve shows the loss of the original queries and the masked queries without completion. Completing the masked queries by the proposed Completion Network improves the learning significantly.

Effect of Completion. We also validate the effect of completion by comparing the loss of the completed queries and the original queries (**red**) with the loss of the masked queries and the original queries (**blue**). As Figure 6 shows, the training loss while including the Completion Network drops much faster than the training loss without including the Completion Network, demonstrating that the Completion Network helps acquire occlusion-tolerant representations effectively by learning to reconstruct the masked queries.

5 Limitations

The proposed MonoMAE could be improved in several aspects. Specifically, MonoMAE leverages depth-aware masking to mask non-occluded queries to simulate object occlusions in the feature space. However, the masked queries may have different patterns as compared with the features of naturally occluded object queries. Such a gap could affect the mask reconstruction and the completed queries which further affects the learned representations and monocular 3D detection performance. This issue could be mitigated by introducing generative networks that learn distributions from extensive real-world data for generating occlusion patterns that are more similar to natural occlusions. In addition, MonoMAE could be evaluated and analyzed more extensively over larger datasets when they are available.

6 Conclusion

This paper presents MonoMAE, a novel method inspired by the Masked Autoencoders (MAE) to deal with the pervasive occlusion problem in the monocular 3D object detection task. MonoMAE consists of two key designs. The first is a depth-aware masking module, which simulates the occlusion for non-occluded object

queries in the feature level during training. The second is a lightweight completion network, which reconstructs and completes the masked object queries. Quantitative and qualitative experiment results show that MonoMAE learns enhanced 3D representations and achieves superior monocular 3D detection performance for both occluded and non-occluded objects. Moving forward, we plan to investigate generative approaches to simulate natural occlusion patterns for various 3D detection tasks.

References

1. Brazil, G., Liu, X.: M3d-rpn: Monocular 3d region proposal network for object detection. In: Proceedings of the IEEE/CVF International Conference on Computer Vision. pp. 9287–9296 (2019) [3](#), [8](#), [9](#), [13](#)
2. Brazil, G., Pons-Moll, G., Liu, X., Schiele, B.: Kinematic 3d object detection in monocular video. In: Proceedings of the IEEE/CVF European Conference on Computer Vision. pp. 135–152. Springer (2020) [9](#)
3. Caesar, H., Bankiti, V., Lang, A.H., Vora, S., Liong, V.E., Xu, Q., Krishnan, A., Pan, Y., Baldan, G., Beijbom, O.: nuscenes: A multimodal dataset for autonomous driving. In: Proceedings of the IEEE/CVF Conference on Computer Vision and Pattern Recognition. pp. 11621–11631 (2020) [8](#)
4. Carion, N., Massa, F., Synnaeve, G., Usunier, N., Kirillov, A., Zagoruyko, S.: End-to-end object detection with transformers. In: Proceedings of the IEEE/CVF European Conference on Computer Vision. pp. 213–229. Springer (2020) [6](#)
5. Chen, A., Zhang, K., Zhang, R., Wang, Z., Lu, Y., Guo, Y., Zhang, S.: Pimae: Point cloud and image interactive masked autoencoders for 3d object detection. In: Proceedings of the IEEE/CVF Conference on Computer Vision and Pattern Recognition. pp. 5291–5301 (2023) [4](#)
6. Chen, H., Huang, Y., Tian, W., Gao, Z., Xiong, L.: Monorun: Monocular 3d object detection by reconstruction and uncertainty propagation. In: Proceedings of the IEEE/CVF Conference on Computer Vision and Pattern Recognition. pp. 10379–10388 (2021) [3](#), [9](#)
7. Chen, X., Kundu, K., Zhang, Z., Ma, H., Fidler, S., Urtasun, R.: Monocular 3d object detection for autonomous driving. In: Proceedings of the IEEE/CVF Conference on Computer Vision and Pattern Recognition. pp. 2147–2156 (2016) [3](#), [8](#)
8. Chen, Y., Tai, L., Sun, K., Li, M.: Monopair: Monocular 3d object detection using pairwise spatial relationships. In: Proceedings of the IEEE/CVF Conference on Computer Vision and Pattern Recognition. pp. 12093–12102 (2020) [3](#), [4](#), [9](#)
9. Chong, Z., Ma, X., Zhang, H., Yue, Y., Li, H., Wang, Z., Ouyang, W.: Monodistill: Learning spatial features for monocular 3d object detection. International Conference on Learning Representations (2022) [9](#)
10. Chu, H., Mo, L., Wang, R., Hu, T., Ma, H.: Visibility of points: Mining occlusion cues for monocular 3d object detection. Neurocomputing **502**, 48–56 (2022) [3](#)
11. Ding, M., Huo, Y., Yi, H., Wang, Z., Shi, J., Lu, Z., Luo, P.: Learning depth-guided convolutions for monocular 3d object detection. In: Proceedings of the IEEE/CVF Conference on Computer Vision and Pattern Recognition. pp. 1000–1001 (2020) [3](#), [9](#)

12. Duan, K., Bai, S., Xie, L., Qi, H., Huang, Q., Tian, Q.: Centernet: Keypoint triplets for object detection. In: Proceedings of the IEEE/CVF International Conference on Computer Vision. pp. 6569–6578 (2019) [3](#)
13. Geiger, A., Lenz, P., Urtasun, R.: Are we ready for autonomous driving? the kitti vision benchmark suite. In: Proceedings of the IEEE/CVF Conference on Computer Vision and Pattern Recognition. pp. 3354–3361. IEEE (2012) [6](#), [8](#), [9](#)
14. Girshick, R.: Fast r-cnn. In: Proceedings of the IEEE/CVF International Conference on Computer Vision. pp. 1440–1448 (2015) [8](#)
15. He, K., Chen, X., Xie, S., Li, Y., Dollár, P., Girshick, R.: Masked autoencoders are scalable vision learners. In: Proceedings of the IEEE/CVF Conference on Computer Vision and Pattern Recognition. pp. 16000–16009 (2022) [2](#), [4](#)
16. He, K., Zhang, X., Ren, S., Sun, J.: Deep residual learning for image recognition. In: Proceedings of the IEEE/CVF Conference on Computer Vision and Pattern Recognition. pp. 770–778 (2016) [9](#)
17. He, T., Soatto, S.: Mono3d++: Monocular 3d vehicle detection with two-scale 3d hypotheses and task priors. In: Proceedings of the AAAI Conference on Artificial Intelligence. vol. 33, pp. 8409–8416 (2019) [3](#)
18. Hu, H.N., Cai, Q.Z., Wang, D., Lin, J., Sun, M., Krahenbuhl, P., Darrell, T., Yu, F.: Joint monocular 3d vehicle detection and tracking. In: Proceedings of the IEEE/CVF International Conference on Computer Vision. pp. 5390–5399 (2019) [3](#)
19. Huang, K.C., Wu, T.H., Su, H.T., Hsu, W.H.: Monodtr: Monocular 3d object detection with depth-aware transformer. In: Proceedings of the IEEE/CVF Conference on Computer Vision and Pattern Recognition. pp. 4012–4021 (2022) [3](#), [9](#), [13](#)
20. Jia, J., Li, Z., Shi, Y.: Monouni: A unified vehicle and infrastructure-side monocular 3d object detection network with sufficient depth clues. In: Advances in Neural Information Processing Systems (2023) [8](#), [9](#), [13](#)
21. Jiang, X., Jin, S., Lu, L., Zhang, X., Lu, S.: Weakly supervised monocular 3d detection with a single-view image. In: Proceedings of the IEEE/CVF Conference on Computer Vision and Pattern Recognition (2024) [3](#)
22. Kumar, A., Brazil, G., Corona, E., Parchami, A., Liu, X.: Deviant: Depth equivariant network for monocular 3d object detection. In: Proceedings of the IEEE/CVF European Conference on Computer Vision. pp. 664–683. Springer (2022) [8](#), [9](#), [13](#)
23. Lang, A.H., Vora, S., Caesar, H., Zhou, L., Yang, J., Beijbom, O.: Pointpillars: Fast encoders for object detection from point clouds. In: Proceedings of the IEEE/CVF Conference on Computer Vision and Pattern Recognition. pp. 12697–12705 (2019) [1](#)
24. Li, Z., Wang, W., Li, H., Xie, E., Sima, C., Lu, T., Qiao, Y., Dai, J.: Bevformer: Learning bird’s-eye-view representation from multi-camera images via spatiotemporal transformers. In: Proceedings of the IEEE/CVF European Conference on Computer Vision. pp. 1–18. Springer (2022) [1](#)
25. Liu, H., Liu, H., Wang, Y., Sun, F., Huang, W.: Fine-grained multilevel fusion for anti-occlusion monocular 3d object detection. IEEE Transactions on Image Processing **31**, 4050–4061 (2022) [3](#), [4](#)
26. Liu, X., Xue, N., Wu, T.: Learning auxiliary monocular contexts helps monocular 3d object detection. In: Proceedings of the AAAI Conference on Artificial Intelligence. vol. 36, pp. 1810–1818 (2022) [9](#)
27. Liu, Y., Wang, T., Zhang, X., Sun, J.: Petr: Position embedding transformation for multi-view 3d object detection. In: Proceedings of the IEEE/CVF European Conference on Computer Vision. pp. 531–548. Springer (2022) [1](#)

28. Liu, Z., Wu, Z., Tóth, R.: Smoke: Single-stage monocular 3d object detection via keypoint estimation. In: Proceedings of the IEEE/CVF Conference on Computer Vision and Pattern Recognition Workshops. pp. 996–997 (2020) [9](#)
29. Liu, Z., Zhou, D., Lu, F., Fang, J., Zhang, L.: Autoshape: Real-time shape-aware monocular 3d object detection. In: Proceedings of the IEEE/CVF International Conference on Computer Vision. pp. 15641–15650 (2021) [3](#), [9](#)
30. Loshchilov, I., Hutter, F.: Decoupled weight decay regularization. International Conference on Learning Representations (2018) [9](#)
31. Lu, Y., Ma, X., Yang, L., Zhang, T., Liu, Y., Chu, Q., Yan, J., Ouyang, W.: Geometry uncertainty projection network for monocular 3d object detection. In: Proceedings of the IEEE/CVF International Conference on Computer Vision. pp. 3111–3121 (2021) [2](#), [3](#), [8](#), [9](#), [13](#)
32. Ma, X., Liu, S., Xia, Z., Zhang, H., Zeng, X., Ouyang, W.: Rethinking pseudo-lidar representation. In: Proceedings of the IEEE/CVF European Conference on Computer Vision. pp. 311–327. Springer (2020) [9](#)
33. Ma, X., Wang, Z., Li, H., Zhang, P., Ouyang, W., Fan, X.: Accurate monocular 3d object detection via color-embedded 3d reconstruction for autonomous driving. In: Proceedings of the IEEE/CVF International Conference on Computer Vision. pp. 6851–6860 (2019) [3](#)
34. Ma, X., Zhang, Y., Xu, D., Zhou, D., Yi, S., Li, H., Ouyang, W.: Delving into localization errors for monocular 3d object detection. In: Proceedings of the IEEE/CVF Conference on Computer Vision and Pattern Recognition. pp. 4721–4730 (2021) [3](#), [9](#)
35. Min, C., Xiao, L., Zhao, D., Nie, Y., Dai, B.: Occupancy-mae: Self-supervised pre-training large-scale lidar point clouds with masked occupancy autoencoders. IEEE Transactions on Intelligent Vehicles (2023) [4](#)
36. Murthy, J.K., Krishna, G.S., Chhaya, F., Krishna, K.M.: Reconstructing vehicles from a single image: Shape priors for road scene understanding. In: International Conference on Robotics and Automation. pp. 724–731. IEEE (2017) [3](#)
37. Pang, Y., Wang, W., Tay, F.E., Liu, W., Tian, Y., Yuan, L.: Masked autoencoders for point cloud self-supervised learning. In: Proceedings of the IEEE/CVF European Conference on Computer Vision. pp. 604–621. Springer (2022) [4](#)
38. Park, D., Ambrus, R., Guizilini, V., Li, J., Gaidon, A.: Is pseudo-lidar needed for monocular 3d object detection? In: Proceedings of the IEEE/CVF International Conference on Computer Vision. pp. 3142–3152 (2021) [9](#)
39. Peng, L., Wu, X., Yang, Z., Liu, H., Cai, D.: Did-m3d: Decoupling instance depth for monocular 3d object detection. In: Proceedings of the IEEE/CVF European Conference on Computer Vision. pp. 71–88. Springer (2022) [3](#), [9](#)
40. Qin, Z., Wang, J., Lu, Y.: Monogrnet: A general framework for monocular 3d object detection. IEEE Transactions on Pattern Analysis and Machine Intelligence **44**(9), 5170–5184 (2021) [3](#)
41. Reading, C., Harakeh, A., Chae, J., Waslander, S.L.: Categorical depth distribution network for monocular 3d object detection. In: Proceedings of the IEEE/CVF Conference on Computer Vision and Pattern Recognition. pp. 8555–8564 (2021) [3](#), [9](#)
42. Ren, S., He, K., Girshick, R., Sun, J.: Faster r-cnn: Towards real-time object detection with region proposal networks. Advances in Neural Information Processing Systems **28** (2015) [3](#)
43. Shi, X., Ye, Q., Chen, X., Chen, C., Chen, Z., Kim, T.K.: Geometry-based distance decomposition for monocular 3d object detection. In: Proceedings of the

- IEEE/CVF International Conference on Computer Vision. pp. 15172–15181 (2021) [8](#), [9](#), [13](#)
44. Simonelli, A., Bulo, S.R., Porzi, L., López-Antequera, M., Kotschieder, P.: Disentangling monocular 3d object detection. In: Proceedings of the IEEE/CVF International Conference on Computer Vision. pp. 1991–1999 (2019) [8](#)
 45. Su, Y., Di, Y., Zhai, G., Manhardt, F., Rambach, J., Busam, B., Stricker, D., Tombari, F.: Opa-3d: Occlusion-aware pixel-wise aggregation for monocular 3d object detection. *IEEE Robotics and Automation Letters* **8**(3), 1327–1334 (2023) [3](#)
 46. Wang, L., Du, L., Ye, X., Fu, Y., Guo, G., Xue, X., Feng, J., Zhang, L.: Depth-conditioned dynamic message propagation for monocular 3d object detection. In: Proceedings of the IEEE/CVF Conference on Computer Vision and Pattern Recognition. pp. 454–463 (2021) [9](#)
 47. Wang, T., Zhu, X., Pang, J., Lin, D.: Fcos3d: Fully convolutional one-stage monocular 3d object detection. In: Proceedings of the IEEE/CVF International Conference on Computer Vision. pp. 913–922 (2021) [8](#)
 48. Wang, Y., Chao, W.L., Garg, D., Hariharan, B., Campbell, M., Weinberger, K.Q.: Pseudo-lidar from visual depth estimation: Bridging the gap in 3d object detection for autonomous driving. In: Proceedings of the IEEE/CVF Conference on Computer Vision and Pattern Recognition. pp. 8445–8453 (2019) [3](#)
 49. Wu, Z., Gan, Y., Wang, L., Chen, G., Pu, J.: Monopgc: Monocular 3d object detection with pixel geometry contexts. *International Conference on Robotics and Automation* (2023) [3](#), [9](#)
 50. Wu, Z., Wu, Y., Pu, J., Li, X., Wang, X.: Attention-based depth distillation with 3d-aware positional encoding for monocular 3d object detection. *Proceedings of the AAAI Conference on Artificial Intelligence* (2023) [3](#)
 51. Xu, J., Peng, L., Cheng, H., Li, H., Qian, W., Li, K., Wang, W., Cai, D.: Mononerf: Nerf-like representations for monocular 3d object detection. In: Proceedings of the IEEE/CVF International Conference on Computer Vision. pp. 6814–6824 (2023) [9](#)
 52. Xu, Q., Zhong, Y., Neumann, U.: Behind the curtain: Learning occluded shapes for 3d object detection. In: Proceedings of the AAAI Conference on Artificial Intelligence. vol. 36, pp. 2893–2901 (2022) [3](#)
 53. Yang, C., Chen, Y., Tian, H., Tao, C., Zhu, X., Zhang, Z., Huang, G., Li, H., Qiao, Y., Lu, L., et al.: Bevformer v2: Adapting modern image backbones to bird’s-eye-view recognition via perspective supervision. In: Proceedings of the IEEE/CVF Conference on Computer Vision and Pattern Recognition. pp. 17830–17839 (2023) [1](#)
 54. Yang, H., He, T., Liu, J., Chen, H., Wu, B., Lin, B., He, X., Ouyang, W.: Gd-mae: generative decoder for mae pre-training on lidar point clouds. In: Proceedings of the IEEE/CVF Conference on Computer Vision and Pattern Recognition. pp. 9403–9414 (2023) [4](#)
 55. Yao, H., Chen, J., Wang, Z., Wang, X., Han, P., Chai, X., Qiu, Y.: Occlusion-aware plane-constraints for monocular 3d object detection. *IEEE Transactions on Intelligent Transportation Systems* (2023) [3](#)
 56. Yin, T., Zhou, X., Krahenbuhl, P.: Center-based 3d object detection and tracking. In: Proceedings of the IEEE/CVF Conference on Computer Vision and Pattern Recognition. pp. 11784–11793 (2021) [1](#)
 57. Zhang, R., Qiu, H., Wang, T., Xu, X., Guo, Z., Qiao, Y., Gao, P., Li, H.: Monodetr: Depth-aware transformer for monocular 3d object detection. *Proceedings of the IEEE/CVF International Conference on Computer Vision* (2023) [2](#), [3](#), [8](#), [9](#), [13](#)

58. Zhang, R., Wang, L., Qiao, Y., Gao, P., Li, H.: Learning 3d representations from 2d pre-trained models via image-to-point masked autoencoders. In: Proceedings of the IEEE/CVF Conference on Computer Vision and Pattern Recognition. pp. 21769–21780 (2023) [4](#)
59. Zhang, Y., Lu, J., Zhou, J.: Objects are different: Flexible monocular 3d object detection. In: Proceedings of the IEEE/CVF Conference on Computer Vision and Pattern Recognition. pp. 3289–3298 (2021) [9](#)
60. Zhou, Y., Tuzel, O.: Voxelnet: End-to-end learning for point cloud based 3d object detection. In: Proceedings of the IEEE/CVF Conference on Computer Vision and Pattern Recognition. pp. 4490–4499 (2018) [1](#)
61. Zhou, Y., He, Y., Zhu, H., Wang, C., Li, H., Jiang, Q.: Monoef: Extrinsic parameter free monocular 3d object detection. *IEEE Transactions on Pattern Analysis and Machine Intelligence* **44**(12), 10114–10128 (2021) [3](#)
62. Zhou, Y., Zhu, H., Liu, Q., Chang, S., Guo, M.: Monoatt: Online monocular 3d object detection with adaptive token transformer. Proceedings of the IEEE/CVF Conference on Computer Vision and Pattern Recognition (2023) [3](#)